

GSIFN: A Graph-Structured and Interlaced-Masked Multimodal Transformer-based Fusion Network for Multimodal Sentiment Analysis

Yijie Jin

School of Computer Engineering and Science
Shanghai University
jyj2431567@shu.edu.cn

Abstract

Multimodal Sentiment Analysis (MSA) leverages multiple data modals to analyze human sentiment. Existing MSA models generally employ cutting-edge multimodal fusion and representation learning-based methods to promote MSA capability. However, there are two key challenges: (i) in existing multimodal fusion methods, the decoupling of modal combinations and tremendous parameter redundancy, lead to insufficient fusion performance and efficiency; (ii) a challenging trade-off exists between representation capability and computational overhead in unimodal feature extractors and encoders. Our proposed GSIFN incorporates two main components to solve these problems: (i) a graph-structured and interlaced-masked multimodal Transformer. It adopts the Interlaced Mask mechanism to construct robust multimodal graph embedding, achieve all-modal-in-one Transformer-based fusion, and greatly reduce the computational overhead; (ii) a self-supervised learning framework with low computational overhead and high performance, which utilizes a parallelized LSTM with matrix memory to enhance non-verbal modal features for unimodal label generation. Evaluated on the MSA datasets CMU-MOSI, CMU-MOSEI, and CH-SIMS, GSIFN demonstrates superior performance with significantly lower computational overhead compared with previous state-of-the-art models.

1 Introduction

With the increasingly widespread use of social media, in which users express sentiment through information forms including text, video, audio, etc. To achieve more natural human-computer interactions, multimodal sentiment analysis (MSA) has become a popular research area (Gandhi et al., 2023). MSA task relies on at least two data modals for sentiment polarity prediction. Specifically, its data form is usually a trimodal combination of text, vision, and audio. The main challenge of MSA is to integrate

heterogeneous data containing different sentiment information, thus achieving semantic disambiguation and effective sentiment analysis. Methods of MSA involve designing effective fusion strategies (Zadeh et al., 2017; Tsai et al., 2019a; Zhang et al., 2023; Zheng et al., 2024) to integrate heterogeneous data for comprehensive sentiment representation and semantic alignment, and developing representation learning strategies (Yu et al., 2021; Yang et al., 2023; Lin and Hu, 2024) to enhance unimodal information and model robustness.

Despite achieving some successes, existing approaches still face two main challenges. First, for the models that focus on multimodal fusion, the computational overhead rises due to the widespread use of cross-modal attention mechanism-based (CMA-based) modules. What is more, different unidirectional bimodal combinations are inputted into multiple independent CMA-based modules for fusion, which prevents such models from fully integrating and fusing trimodal representation information. Instead, they over-retain redundant information in the dominant modals of bimodal combinations. Therefore, these models are excessively redundant and in need of pruning. Previous models like MISA (Hazarika et al., 2020) and AcFormer (Zong et al., 2023) apply naive serial weight-sharing strategy and bottle-neck mechanism to share trimodal representation information and prune the model. However, these methods lead to information disorder, which disperses attention weight or over-loses fine-grained information. Second, for the representation learning-based models, feature extraction and encoding modules of non-verbal modals cannot effectively balance the computational overhead and representation performance. Vanilla models (GRU (Chung et al., 2014), LSTM (Hochreiter, 1997), etc.) and conventional extractors (OpenFace2.0 (Baltrusaitis et al., 2018), COVAREP (Degottex et al., 2014), etc.) usually cause excessive loss of non-verbal modal

representation capability. In contrast, large and advanced models (ViT(Dosovitskiy et al., 2021), Wav2Vec(Schneider et al., 2019), etc.) bring superior performance but incur excessive computational overhead.

To address the aforementioned issues, we propose a model called **Graph-Structured and Interlaced-Masked Multimodal Transformer-based Fusion Network**, dubbed **GSIFN**. There are two attractive properties in GSIFN. First, in the process of multimodal fusion, GSIFN achieves efficient and low-computational-overhead sentiment representation information sharing without information disorder. To attain this, we design GsiT, a Graph-structured and interlaced-masked multimodal Transformer. Organized into modal subgraphs, GsiT employs the Interlaced Mask (IM) mechanism to create Multimodal Graph Embeddings (MGE). The Interlaced-Inter-Fusion Mask (IFM) constructs fusion MGE by generating two opposing unidirectional ring MGEs, utilizes shared information for complete and comprehensive fusion. The Interlaced-Intra-Enhancement Mask (IEM) generates enhancement MGE to optimize and enhance fused features. IM leverages a novel weight-sharing strategy to enable an all-modal-in-one fusion and enhancement mechanism effectively. Eliminating redundant information and achieving pruning enhances fusion effectiveness and efficiency. Second, GSIFN significantly reduces computational overhead brought by non-verbal modal feature enhancement operations and ensures the robustness and MSA performance of the model. We employ a unimodal label generation module (ULGM) to enhance the model robustness and apply an extended LSTM with matrix memory (mLSTM) to enhance non-verbal modal features for ULGM. Thus, the computational overhead and the representation capability of GSIFN are balanced. Overall, our contributions are as follows:

- We propose GSIFN, a graph-structured and interlaced-masked multimodal Transformer-based fusion network. Multiple and comprehensive experiments on CMU-MOSI(Zadeh et al., 2016), CMU-MOSEI(Bagher Zadeh et al., 2018), and CH-SIMS(Yu et al., 2020) validate its effectiveness and superiority.
- We design GsiT, a graph-structured and interlaced-masked multimodal Transformer that uses the Interlaced Mask mechanism to build multimodal graph embeddings in units of modal subgraphs. It ensures efficient and

effective information sharing, reduces spatio-temporal redundancy and noise, and yields a more compact and informative multimodal representation while lowering the module’s parameter count and computational overhead.

- We employ mLSTM, an extended LSTM with matrix memory, to enhance non-verbal modal features utilized for unimodal label generation. This approach improves model robustness and representation capability and avoids the overhead of large models.

2 Related Work

2.1 Multimodal Sentiment Analysis

Multimodal sentiment analysis (MSA) is an increasingly popular research field. MSA data form is typically a combination of more than two modals. Specifically, the most widely used form is a trimodal combination of text, vision, and audio. Earlier MSA models focus on modal fusion. Zadeh et al. (2016) are among the first promoters in this field. TFN (Zadeh et al., 2017), LMF (Liu et al., 2018), and MFN(Zadeh et al., 2018) proposed by them are among the earliest to enhance the MSA performance by designing complex structures and advanced fusion methods.

With the rise of Transformer(Vaswani et al., 2017), Tsai et al. (2019a) proposes MulT which utilizes the cross-modal attention mechanism (CMA) from the perspective of modal translation. CMA can effectively integrate multimodal data while realizing implicit modal alignment. Based on MulT and CMA, models such as TETFN (Wang et al., 2023a) and ALMT (Zhang et al., 2023) focus on text data to enhance non-verbal modal data, for text data contains stronger sentiment information. Thus, they achieve superior representation and fusion capability.

MAG-BERT (Rahman et al., 2020) uses a Multimodal Adaptation Gate (MAG) to fine-tune BERT (Devlin et al., 2019) using multimodal data. Based on MAG-BERT, CENet(Wang et al., 2023b), HyCon(Mai et al., 2023), and AOBERT(Kim and Park, 2023), propose novel gating mechanisms or enhanced multimodal representation techniques to improve MSA capability of BERT.

To improve the robustness and the representation capability of existing models, thereby improving the overall MSA capability of them, representation learning-based models such as MFM (Tsai et al., 2019b), Self-MM (Yu et al., 2021), Con-

FEDE (Yang et al., 2023), and MTMD (Lin and Hu, 2024) are proposed. These models use the multi-loss strategy, self-supervised learning, contrastive learning, and knowledge distillation to achieve a robust representation of intra- and inter-modal information. As a result, they have shown outstanding performance in MSA tasks.

By combining multimodal Transformers and representation learning, models such as TETFN, MMML(Wu et al., 2024), and AcFormer(Zong et al., 2023) have achieved remarkable performance promotion. These findings suggest that the combination of these two techniques can fully exploit their respective strengths altogether.

Overuse of multimodal Transformers with large parameters limits the efficiency of these methods. In addition, feeding different fusion combinations into multiple separate Transformers results in insufficient information interaction and uneven weight distribution. To address these issues, inspired by graph attention networks (Velickovic et al., 2018; Brody et al., 2022), we propose a graph-structured multimodal Transformer with modal subgraph units.

2.2 Linear Attention Networks

In the field of natural language processing (NLP), avoiding the computational overhead of Transformers while maintaining performance has become a popular research topic. RWKV (Peng et al., 2023a), RetNet (Sun et al., 2023), Mamba (Gu and Dao, 2023), Mamba-2 (Dao and Gu, 2024), and xLSTM (Pöppel et al., 2024) are representatives among them. As an extended LSTM, xLSTM introduces an exponential gating mechanism to solve the limitations of memory capacity and parallelization.

Meanwhile, recent works of MSA have begun to use more advanced feature extractors and encoders to capture non-verbal modal features with superior representation capability. For instance, TETFN and AcFormer use Vision Transformer (ViT) (Dosovitskiy et al., 2021) to extract vision features, AcFormer uses Wav2Vec2.0 (Baevski et al., 2020) to extract audio features, and MMML fine-tunes Data2Vec (audio)(Baevski et al., 2022). However, these methods often result in excessive growth in parameter count, with obscure improvement over features extracted from traditional methods. In GSIFN, variation mLSTM of xLSTM is used to enhance the non-verbal feature for unimodal label generation, it significantly reduces the computational overhead and ensures model performance.

3 Methodology

3.1 Preliminaries

The objective of multimodal sentiment analysis (MSA) is to define sentiment polarity using multimodal data. Existing MSA datasets generally contain three modals: t, v, a represent text, vision, and audio, respectively. In particular, m denotes multimodal which fuses t, v, a . The input of MSA task is $\mathbf{S}_u \in \mathbb{R}^{T_u^s \times d_u^s}$, where $u \in \{t, v, a\}$, T_u^s denotes the raw sequence length and d_u^s denotes the raw representation dimension of modal u . In this paper, we define multiple outputs $\hat{y}_u \in R$, where $u \in \{t, v, a, m\}$, $\hat{y}_{\{t,v,a\}}$ denote unimodal outputs, obtained for unimodal label generation. \hat{y}_m denotes the fusion output, obtained for the final prediction. Other symbols are defined as follows, fusion module inputs are $\mathbf{X}_u \in \mathbb{R}^{T_u \times d_u}$, where $u \in \{t, v, a\}$, T_u denotes the sequence length and d_u denotes the representation dimension of modal u . ULGM inputs are $\mathcal{X}_u \in \mathbb{R}^{T_u \times d_u}$, where $u \in \{m, t, v, a\}$. \mathcal{X}_m is the input feature of predictor. In particular, in the interpretation of GsiT, $\mathbf{X}_{\{t,v,a\}}$ are abstracted to vertex sequences $\mathcal{V}_{\{t,v,a\}}$. Labels are denoted as $y_u \in R$, where $u \in \{t, v, a, m\}$, $y_{\{t,v,a\}}$ are unimodal labels generated by ULGM, y_m is the ground truth label for fusion output.

3.2 Overall Architecture

The overall architecture of GSIFN is shown in Figure 1, which comprises three main components: (i) *Modal Encoding* employs tokenizers (for text), feature extractors, and temporal enhancers (for non-verbal modals vision&audio) to encode raw multimodal data into feature sequences. Enhanced non-verbal features are used for unimodal label generation; (ii) *Graph-Structured Multimodal Fusion* takes encoded text, vision, and audio embeddings as input. The core graph-structured Transformer-based fusion module constructs multimodal graph embeddings using interlaced masks. Weight-sharing is used to promote modal interaction, reduce redundant parameters, enhance fusion efficiency, and prune the model; (iii) *Self-Supervised Learning Framework* produces final representations by projecting text features, enhanced vision/audio features, and fusion output to hidden states, defining positive and negative centers, and generating unimodal labels from unimodal hidden states.

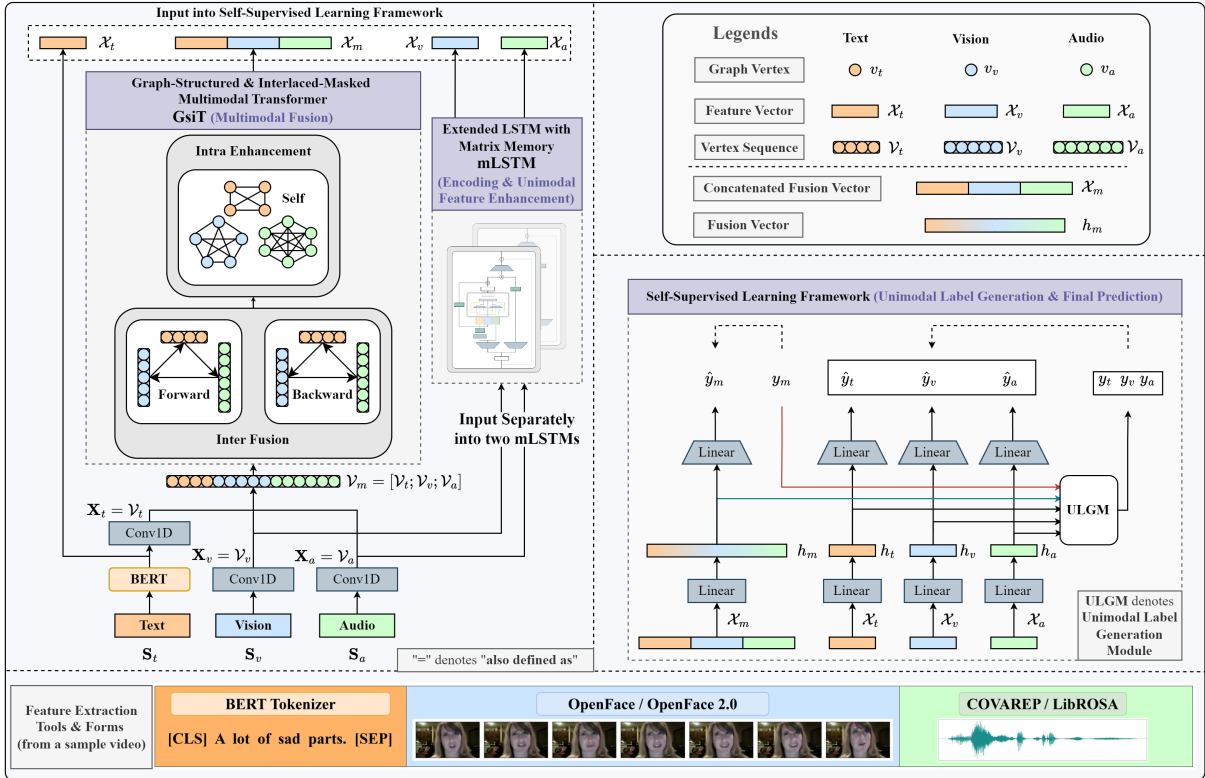


Figure 1: GSIFN Architecture. Note: The detailed structure of GsiT, mLSTM is in Figure 2, 7.

3.3 Modal Encoding

For text modal, we use the pretrained Transformer BERT as the text encoder. Input text token sequence is constructed by the raw sentence $\mathbf{S}_t = \{w_1, w_2, \dots, w_n\}$ concatenated with two special tokens ([CLS] at the head and [SEP] at the end) which form $\mathbf{S}'_t = \{[\text{CLS}], w_1, w_2, \dots, w_n, [\text{SEP}]\}$. Then input \mathbf{S}'_t into BERT to construct \mathcal{X}_t , which is used to generate text modal labels.

$$\mathcal{X}_t = \text{BERT}(\mathbf{S}'_t) = \{t_0, t_1, \dots, t_{n+1}\} \quad (1)$$

Following previous works (Tsai et al., 2019a; Wang et al., 2023a), input sequences $\mathbf{X}_{\{t,v,a\}}$ are handled by one dimension convolution (Conv1D) layer from \mathcal{X}_t and raw vision, audio sequences $\mathbf{S}_{\{v,a\}}$ to construct low-level features.

$$\mathbf{X}_t = \text{Conv1D}(\mathcal{X}_t) \quad (2)$$

$$\mathbf{X}_{\{v,a\}} = \text{Conv1D}(\mathbf{S}_{\{v,a\}}) \quad (3)$$

We then use an extended LSTM (Pöppel et al., 2024) with matrix memory and a covariance update rule (mLSTM) as the temporal enhancer for vision and audio modals. mLSTM provides an improved memory mechanism over vanilla LSTM, allowing

for deeper semantic mining of non-verbal modals while reducing computational overhead. For a detailed definition of mLSTM, see Appendix F.2.

mLSTM is used to enhance the temporal features of vision and audio.

$$\mathcal{X}_{\{v,a\}} = \text{mLSTM}(\mathbf{X}_{\{v,a\}}) \quad (4)$$

mLSTM can enhance non-verbal modal features utilized for unimodal label generation.

3.4 Graph-Structured Multimodal Fusion

Following previous works (Tsai et al., 2019a; Wang et al., 2023a), we only use the low-level temporal feature sequences $\mathbf{X}_{\{t,v,a\}}$ as input of multimodal fusion. $\mathbf{X}_{\{t,v,a\}}$ are regarded as graph vertex sequences $\mathcal{V}_{\{t,v,a\}}$. Then, concatenate vertices into a single sequence $\mathcal{V}_m = [\mathcal{V}_t; \mathcal{V}_v; \mathcal{V}_a]^\top$. \mathcal{V}_m is treated as the multimodal graph embedding (MGE). We define $\mathcal{W}_u \in \mathbb{R}^{T_u \times d_u^f}$ and $\mathcal{W}_u^b \in \mathbb{R}^{T_u \times d_u^f}$, where $u \in \{q, k, v\}$, d_u^f is the attention feature dimension, as the query, key, value projection weight of \mathcal{V}_m and \mathcal{V}_m^b . The architecture of graph-structured and interlaced-masked multimodal Transformer (GsiT) architecture is shown in Figure 2.

Graph Structure Construction To start with, we utilize the self-attention mechanism as the basic

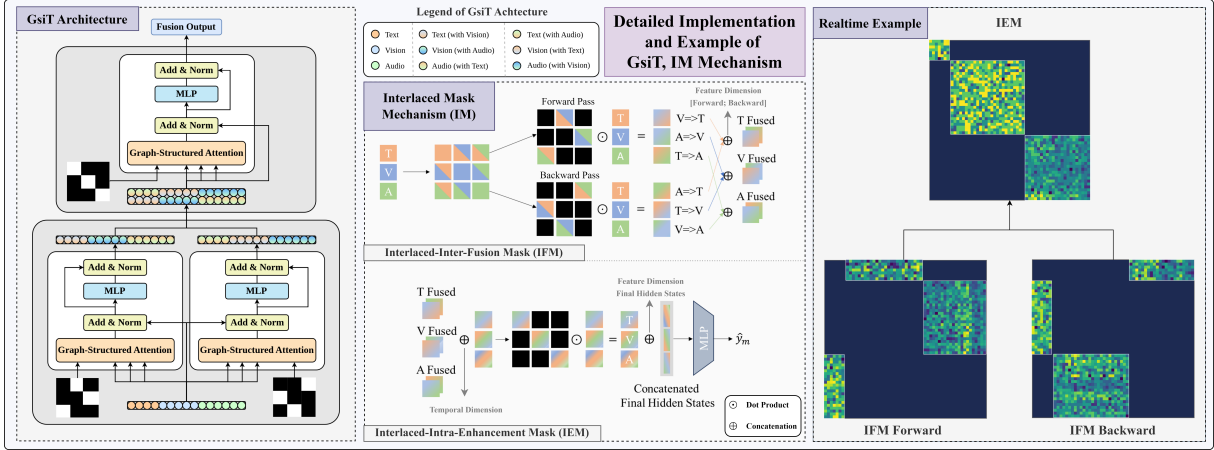


Figure 2: GsiT Architecture and IM Mechanism.

theory to construct a naive fully connected graph. The attention weight matrix is regarded as the adjacency matrix \mathcal{A} with dynamic weights. In \mathcal{A} , $\mathcal{E}^{i,j} \in \mathbb{R}^{T_i \times T_j}$, $\{i, j\} \in \{t, v, a\}$ is the adjacency matrix of the subgraph constructed by \mathcal{V}_i and \mathcal{V}_j .

$$\begin{aligned} \mathcal{A} &= (\mathcal{W}_q \mathcal{V}_m) \cdot (\mathcal{W}_k \mathcal{V}_m)^\top \\ &= \begin{pmatrix} \mathcal{E}^{t,t} & \mathcal{E}^{t,v} & \mathcal{E}^{t,a} \\ \mathcal{E}^{v,t} & \mathcal{E}^{v,v} & \mathcal{E}^{v,a} \\ \mathcal{E}^{a,t} & \mathcal{E}^{a,v} & \mathcal{E}^{a,a} \end{pmatrix} \end{aligned} \quad (5)$$

The derivation process of detailed graph structure construction (from vertex to subgraph) is in Appendix D.1.

Interlaced Mask Mechanism Interlaced Mask (IM) is a modal-wise mask mechanism, thus all of the elements in the mask matrix are subgraph adjacency matrices. The mask matrix is represented as a block matrix. IM ensures all-modal-in-one fusion without information disorder. The computation procedure with IM is shown in Figure 2. The explanation of the information disorder caused by the concatenation operation of multimodal sequences is in Appendix D.2.

To start with, to avoid the influence of intra-modal subgraph $\mathcal{E}_{i \in \{t, v, a\}}^{i,i}$, we apply modal-wise intra mask as shown in Equation 6. We define $\mathcal{O}^{i,j} \in \mathbb{R}^{T_i \times T_j}$ as all zero matrix, $\mathcal{J}^{i,j} \in \mathbb{R}^{T_i \times T_j}$ as all negative infinity matrix.

$$\mathcal{M}_{inter} = \begin{pmatrix} \mathcal{J}^{t,t} & \mathcal{O}^{t,v} & \mathcal{O}^{t,a} \\ \mathcal{O}^{v,t} & \mathcal{J}^{v,v} & \mathcal{O}^{v,a} \\ \mathcal{O}^{a,t} & \mathcal{O}^{a,v} & \mathcal{J}^{a,a} \end{pmatrix} \quad (6)$$

\mathcal{M}_{inter} can already make multimodal fusion not be affected by intra-modal subgraphs. However, different modal sequences are still recognized as

the same sequence. Therefore, we extend \mathcal{M}_{inter} to the following two mask matrices, which is called as Interlaced-Inter-Fusion Mask (IFM).

$$\begin{cases} \mathcal{M}_{inter}^{forward} = \begin{pmatrix} \mathcal{J}^{t,t} & \mathcal{O}^{t,v} & \mathcal{J}^{t,a} \\ \mathcal{J}^{v,t} & \mathcal{J}^{v,v} & \mathcal{O}^{v,a} \\ \mathcal{O}^{a,t} & \mathcal{J}^{a,v} & \mathcal{J}^{a,a} \end{pmatrix} \\ \mathcal{M}_{inter}^{backward} = \begin{pmatrix} \mathcal{J}^{t,t} & \mathcal{J}^{t,v} & \mathcal{O}^{t,a} \\ \mathcal{O}^{v,t} & \mathcal{J}^{v,v} & \mathcal{J}^{v,a} \\ \mathcal{J}^{a,t} & \mathcal{O}^{a,v} & \mathcal{J}^{a,a} \end{pmatrix} \end{cases} \quad (7)$$

Based on the two matrices, two opposing unidirectional ring graphs can be constructed to achieve a complete fusion procedure. We define softmax operation as \mathcal{S} , dropout operation as \mathcal{D} , and function composition operator as \circ .

$$\begin{cases} \mathcal{G}_{inter}^{forward} = \mathcal{S} \circ \mathcal{D}(\mathcal{A} + \mathcal{M}_{inter}^{forward}) \\ \mathcal{G}_{inter}^{backward} = \mathcal{S} \circ \mathcal{D}(\mathcal{A} + \mathcal{M}_{inter}^{backward}) \end{cases} \quad (8)$$

By now, $\mathcal{G}_{inter}^{forward}$ and $\mathcal{G}_{inter}^{backward}$ truly make MGE \mathcal{V}_m graph-structured. Both of the two matrices manage to aggregate the information of the trimodal without temporal information disorder and intra-modal information influence. Subsequently, the fusion process is performed.

$$\begin{cases} \bar{\mathcal{V}}_m^{forward} = \mathcal{G}_{inter}^{forward} \mathcal{W}_v \mathcal{V}_m \\ \bar{\mathcal{V}}_m^{backward} = \mathcal{G}_{inter}^{backward} \mathcal{W}_v \mathcal{V}_m \end{cases} \quad (9)$$

As shown in Figure 2, two MGEs are constructed by IFM in two separated Transformers, which are two opposing unidirectional rings. Due to the special structure of them, a complete and comprehensive fusion process is achieved.

After fusion, intra-modal subgraphs need to be enhanced accordingly. Therefore, the Intelaced-Intra-Enhancement Mask (IEM) \mathcal{M}_{intra} is constructed. \mathcal{M}_{intra} leaves only intra-modal subgraphs visible to enhance the fused MGEs.

$$\mathcal{M}_{intra} = \mathcal{J} - \mathcal{M}_{inter} \quad (10)$$

where \mathcal{J} denotes a negative infinity matrix at the same size of \mathcal{M}_{inter} .

Subsequently, concatenate two opposing unidirectional ring MGEs on feature dimension into one bidirectional MGE. We define \parallel as the concatenation operation on the feature dimension.

$$\bar{\mathcal{V}}_m^{bidirection} = \parallel \bar{\mathcal{V}}_m^{\{forward, backward\}} \quad (11)$$

Utilizing the bidirectional MGE $\bar{\mathcal{V}}_m^{bidirection}$ and \mathcal{M}_{intra} , the intra-modal enhancement graph could be constructed. We define $\bar{\mathcal{V}}_m^b = \bar{\mathcal{V}}_m^{bidirection}$.

$$\mathcal{A}_{fusion} = (\mathcal{W}_q^b \bar{\mathcal{V}}_m^b) \cdot (\mathcal{W}_k^b \bar{\mathcal{V}}_m^b)^\top \quad (12)$$

$$\mathcal{G}_{intra} = \mathcal{S} \circ \mathcal{D}(\mathcal{A}_{fusion} + \mathcal{M}_{intra}) \quad (13)$$

Then, we construct the final feature $\bar{\mathcal{V}}_m$.

$$\bar{\mathcal{V}}_m = \mathcal{G}_{intra} \mathcal{W}_v^b \bar{\mathcal{V}}_m^b \quad (14)$$

Finally, as shown in Figure 2, $\bar{\mathcal{V}}_m$ is decomposed according to the length of the original feature sequence. Then, the final hidden states of different modals are concatenated on the feature dimension to construct the fusion feature \mathcal{X}_m .

The detailed generation algorithm of IM is described in Appendix F.1.

3.5 Self-Supervised Learning Framework

A unimodal label generation module (ULGM) is integrated into our approach to capture unimodal-specific information and ensure model robustness. As shown in Figure 1, we use input features $\mathcal{X}_{\{t,v,a\}}$ to generate unimodal final hidden states $h_{\{t,v,a\}}$. During the prediction process, ULGM uses $h_{\{t,v,a\}}$ and ground truth multimodal labels to define positive and negative centers, which are determined based on the predicted unimodal labels and multimodal fusion representations. Next, we calculate the relative distance of each modal representation from the positive and negative centers. Then, we generate new unimodal labels $y_{\{t,v,a\}}^i$ from the unimodal labels to the ground truth multimodal label,

where i represents the i^{th} training iteration. In this way, sentiment analysis can be more conducive to obtaining the distinguishing information of different modals, while maintaining the consistency of each modal. Thus, the robustness of GSIFN is ensured.

Using the predicted results $\hat{y}_{\{m,t,v,a\}}$ and the ground truth multimodal label y_m and the formerly generated labels $y_{\{t,v,a\}}^{i-1}$, we implement a weighted loss to optimize our model. The weighted loss is defined by Equation 15 whereas the unimodal loss for each modal is defined in Equation 16.

$$\mathcal{L}_w = \sum_{u \in \{m,t,v,a\}} \mathcal{L}_u \quad (15)$$

$$\mathcal{L}_u = \frac{\sum_{i=0}^{\mathcal{B}} w_u^i * |\hat{y}_u^i - y_u^i|}{\mathcal{B}} \quad (16)$$

$$w_u^i = \begin{cases} 1 & u = m \\ \tanh(|\hat{y}_u^i - \hat{y}_m^i|) & u \in \{t,v,a\} \end{cases}$$

where \mathcal{B} denotes the appointed batch size.

4 Experiment

We evaluate GSIFN on three widely used datasets, CMU-MOSI (Zadeh et al., 2016), CMU-MOSEI (Bagher Zadeh et al., 2018), and CH-SIMS (Yu et al., 2020). These datasets provide aligned (CMU-MOSI, CMU-MOSEI) and unaligned (all) multimodal data (text, vision, and audio) for each utterance. Further details are in Appendix B.

Following previous works (Yang et al., 2023; Wang et al., 2024; Lin and Hu, 2024), several evaluation metrics are adopted. Binary classification accuracy (Acc-2), F1 Score (F1), three classification accuracy (Acc-3), five classification accuracy (Acc-5), seven classification accuracy (Acc-7), mean absolute error (MAE), and the correlation of the model’s prediction with human (Corr). In particular, Acc-3 and Acc-5 are applied only for CH-SIMS dataset, Acc-2 and F1 are calculated in two ways: negative/non-negative (NN) and negative/positive (NP) on CMU-MOSI and CMU-MOSEI datasets. Acc-2, F1 and Acc-3 reflect coarse-grained capability. Acc-5, Acc-7, MAE, and Corr reflect fine-grained capability.

For CMU-MOSI and CMU-MOSEI, we choose MulT (Tsai et al., 2019a), MTAG (Yang et al., 2021), MISA (Hazarika et al., 2020), HyCon-BERT (Mai et al., 2023), TETFN (Wang et al., 2023a), ConFEDE (Yang et al., 2023), MMIN (Fang et al., 2024),

Table 1: Comparison on CMU-MOSI and CMU-MOSEI.

Model	CMU-MOSI					CMU-MOSEI					Data State
	Acc-2(%) [†]	F1(%) [†]	Acc-7(%) [†]	MAE _↓	Corr [†]	Acc-2(%) [†]	F1(%) [†]	Acc-7(%) [†]	MAE _↓	Corr [†]	
MuT*	83.0 / -	82.8 / -	40.0	0.871	0.698	81.6 / -	81.6 / -	50.7	0.591	0.694	Unaligned
Self-MM*	84.0 / 86.0	84.4 / 86.0	-	<u>0.713</u>	<u>0.798</u>	82.8 / 85.2	82.5 / 85.3	-	<u>0.530</u>	0.765	Unaligned
MTAG*	82.3 / -	82.1 / -	38.9	0.866	0.722	- / -	- / -	-	-	-	Unaligned
MISA*	81.8 / 83.4	81.7 / 83.6	42.3	0.783	0.761	83.6 / 85.5	83.8 / 85.3	52.2	0.555	0.756	Unaligned
HyCon-BERT*	- / 85.2	- / 85.1	46.6	0.713	0.790	- / 85.4	- / 85.6	52.8	0.601	<u>0.776</u>	Aligned
ConFEDE*	<u>84.2 / 85.5</u>	<u>84.1 / 85.5</u>	42.3	0.742	0.784	81.7 / 85.8	82.2 / 85.8	54.9	0.522	0.780	Unaligned
MMIN*	<u>83.5 / 85.5</u>	<u>83.5 / 85.5</u>	-	0.741	0.795	83.8 / 85.9	83.9 / 85.8	-	0.542	0.761	Unaligned
MTMD*	84.0 / 86.0	83.9 / 86.0	<u>47.5</u>	0.705	<u>0.799</u>	<u>84.8 / 86.1</u>	<u>84.9 / 85.9</u>	<u>53.7</u>	<u>0.531</u>	<u>0.767</u>	Unaligned
MuT [†]	79.6 / 81.4	79.1 / 81.0	36.2	0.923	0.686	78.1 / 83.7	78.9 / 83.7	53.4	0.559	0.740	Unaligned
Self-MM [†]	82.2 / 83.5	82.3 / 83.6	43.9	0.758	0.792	80.8 / 85.0	81.3 / 84.9	53.3	0.539	0.761	Unaligned
TETFN [†]	82.4 / 84.0	82.4 / 84.1	46.1	0.749	0.784	81.9 / 84.3	82.1 / 84.1	52.7	0.576	0.728	Unaligned
GSIFN	85.0 / 86.0	85.0 / 86.0	48.3	<u>0.707</u>	0.801	85.0 / 86.3	85.1 / 86.2	<u>53.4</u>	0.538	<u>0.767</u>	Unaligned

Table 2: Comparison on CH-SIMS.

Model	CH-SIMS					
	Acc-2(%) [†]	Acc-3(%) [†]	Acc-5(%) [†]	F1(%) [†]	MAE _↓	Corr [†]
TFN [†]	77.7	<u>66.3</u>	42.7	77.7	0.436	<u>0.582</u>
MFN [†]	77.8	<u>65.4</u>	38.8	77.6	0.443	0.566
MuT [†]	77.8	65.3	38.2	77.7	0.443	0.578
MISA [†]	75.3	62.4	35.5	75.4	0.457	0.553
Self-MM [†]	<u>78.1</u>	65.2	41.3	<u>78.2</u>	<u>0.423</u>	<u>0.585</u>
TETFN [†]	<u>78.0</u>	64.4	<u>42.9</u>	<u>78.0</u>	<u>0.425</u>	<u>0.582</u>
GSIFN	80.5	67.2	45.5	80.7	0.397	0.619

Table 3: Ablation study on CMU-MOSI.

Description	CMU-MOSI				
	Acc-2(%) [†]	F1(%) [†]	Acc-7(%) [†]	MAE _↓	Corr [†]
GSIFN	85.0 / 86.0	85.0 / 86.0	48.3	0.707	0.801
w/o GsiT	83.8 / 85.5	83.2 / 85.7	46.5	0.742	0.790
w/o mLSTM	84.6 / 86.0	84.5 / 86.0	47.2	0.730	0.792
w/o ULGM	83.4 / 84.8	83.4 / 84.8	46.7	0.711	0.801

MTMD(Lin and Hu, 2024), Self-MM(Yu et al., 2021) as baselines. As for CH-SIMS, TFN(Zadeh et al., 2017), MFN(Zadeh et al., 2018), MISA, MuT, Self-MM and TETFN are chosen. All of which are previous state-of-the-arts(SOTA). Further details are in Appendix C.

Experiment settings of hyperparameters and feature extraction methods are in Appendix A.1.

4.1 Results

The performance comparison on all datasets is summarized in Table 1 and Table 2.

For all metrics, the best results are highlighted in bold, the second-best results are double-underlined, and the third-best results are single-underlined. [†] denotes that the model is sourced from the GitHub page¹ and the results are reproduced, * denotes the result is obtained directly from the original paper.

Remarks. GSIFN is trained end-to-end without applying any pertaining, using the unimodal labels of CH-SIMS, and employing pretrained non-verbal

modal encoders like ViT(Dosovitskiy et al., 2021). Thus, all replicated results ensure consistency and fairness in the experimental environment.

In Table 1, for a fair comparison in CMU-MOSI and CMU-MOSEI, we split models into two categories based on data state: Unaligned and Aligned. For Acc-2 and F1, the left of the "/" corresponds to NN and the right corresponds to NP.

As shown in Tables 1 and 2, GSIFN surpasses all previous SOTA models across most metrics in the evaluated datasets. When compared with widely used fusion methods such as MuT, MuT-based models like TETFN and MMIN, and vanilla graph attention network-based model MTAG, GSIFN consistently delivers superior performance across all metrics. This highlights GsiT in GSIFN as one of the leading SOTA fusion methods.

Metrics such as Acc-7 and Corr in CMU-MOSEI, and MAE in CMU-MOSI, demonstrate GSIFN achieving at least third-best performance. Despite Self-MM’s original result Self-MM* showing a higher MAE in CMU-MOSEI compared with GSIFN’s, GSIFN outperforms the reproduced Self-MM[†] in all metrics. Additionally, when compared with advanced representation learning methods like ConFEDE and MTMD, GSIFN exhibits superior performance in most metrics, validating the efficacy of mLSTM in enhancing non-verbal modal features for ULGM.

The relatively weaker performance of GSIFN in CMU-MOSEI can be attributed to the extended sequence lengths of vision and audio modals, which lead to excessive padding and semanticless information, thereby weakening the performance of GSIFN. Further details are in section **Limitations**.

GSIFN achieves effective all-modal-in-one fusion through GsiT and enhances non-verbal modal features for ULGM via mLSTM, resulting in superior performance over previous SOTAs.

¹<https://github.com/thuiar/MMSA>

4.2 Ablation Study

In this section, we discuss the ablation study on modules in Table 3. In Table 3, w/o denotes the absence of the corresponding module in the model. Further ablation study results and analysis are in Appendix A.2

There are three main modules in GSIFN, including GsiT for multimodal fusion, extended mLSTM for vision, audio feature enhancement, and ULGM for self-supervised learning.

The results in Table 3 indicate all the modules are necessary for achieving SOTA performance. GsiT realizes all-modal-in-one Transformer-based fusion, without GsiT, the performance of the whole model has a substantial decrease in all metrics. It is the core module and is especially significant in fine-grained tasks. Without mLSTM, the performance weakens mainly on fine-grained tasks, it is a necessary module. Removing ULGM, the performance weakens on almost all the metrics, especially on coarse-grained tasks, it is irremovable.

4.3 Further Analysis

We discuss the GsiT comparison with MulT on performance and efficiency and further prove the efficiency and effectiveness of mLSTM in this section. Note that Params denotes the number of parameters, and FLOPS denotes floating-point operations per second.

GsiT and MulT For a fair comparison, we trained MulT and GsiT with the same hyperparameters. The results are shown in the Table 4. GsiT outperforms MulT in all metrics. The Params and FLOPS of GsiT are much lower than MulT.

The visual architecture comparison of MulT and GsiT is in Appendix E. MulT mainly uses cross-modal attention to realize effective multimodal fusion. MulT realizes comprehensive fusion and enhancement separately in 9 Transformers. However, GsiT uses IM to make each of the MGE contain trimodal information altogether. It reduces the number of Transformers from 9 to 3. Through weight-sharing without information disorder, each of the Transformers in GsiT can completely fuse trimodal sentiment information all in one, achieving better weight regularization and fusion performance.

Vision/Audio Encoder Efficiency As shown in Table 4, Params and FLOPS of widely used non-verbal modal feature extractors. Vision Transformer (ViT)(Dosovitskiy et al., 2021), Wav2Vec(Schneider et al., 2019), and Whis-

per(Radford et al., 2023) are commonly employed to extract high-quality features. We employ mLSTM to enhance low-quality features extracted by COVAREP(Degottex et al., 2014) (for audio), OpenFace(Baltrusaitis et al., 2016) (for vision). The Params and FLOPS of mLSTMs is way lower than ViT, Wav2Vec and Whisper.

To analyze the efficiency and effectiveness of mLSTM, GSIFN is compared with two models using large model extractors: TETFN, AcFormer. As shown in Table 6, GSIFN performs better than TETFN and AcFormer in most of the metrics.

Table 4: Comparison of GsiT and MulT on CMU-MOSI and CMU-MOSEI.

Model	CMU-MOSI		CMU-MOSEI		Params(M)↓	FLOPS(G)↓
	F1(%)↑	MAE↓	F1(%)↑	MAE↓		
MulT†	79.1 / 81.0	0.923	78.9 / 83.7	0.559	4.362	105.174
GsiT	83.4 / 85.0	0.716	84.4 / 86.3	0.539	0.891	25.983

Table 5: The Computational Overhead of Different Vision/Audio Modal Enhancement Models.

Model	mLSTM(V)	mLSTM(A)	ViT	Wav2Vec	Whisper
Params(M)↓	0.439	0.439	127.272	94.395	17.120
FLOPS(G)↓	1.674	1.252	35.469	68.543	315.128

Table 6: Comparison with model using large model extractors. Note: OF denotes OpenFace, CR denotes COVAREP, and the results are from the original papers.

Model	CMU-MOSI					Extractor(V/A)	Enhancer
	Acc-2(%)↑	F1(%)↑	Acc-7(%)↑	MAE↓	Corr†		
GSIFN	85.0 / 86.0	85.0 / 86.0	48.3	0.707	0.801	OF/CR	mLSTM
TETFN*	84.1 / 86.1	83.8 / 86.1	46.5	0.717	0.800	ViT/CR	LSTM
AcFormer*	82.3 / 85.4	82.1 / 85.2	44.2	0.742	0.794	ViT/Wav2Vec	Transformer

5 Conclusion

In this paper, we propose GSIFN, a graph-structured and interlaced-masked multimodal Transformer-based fusion network. It addresses the challenges of multimodal sentiment analysis (MSA) with two key components: (i) a graph-structured and interlaced-masked multimodal Transformer that builds a robust multimodal graph embedding and achieves efficient, effective all-modal-in-one fusion; (ii) a self-supervised learning framework using mLSTM to enhance non-verbal modal features for unimodal label generation that offers high performance with low cost. The experimental results show that GSIFN reduces the computational overhead and reaches SOTA in MSA.

Limitations

The performance of GSIFN on fine-grained tasks like MAE, Corr, and Acc-7 is worthy of further improvement, which is the major limitation. Moreover, its capability on missing-modal tasks could be further discovered. The potential approaches to further address the major limitations of GSIFN will be discussed in the following paragraphs. As for the missing-modal tasks capability, it is a more complex and distinct extension of the field of MSA, therefore, it can only be discussed in more detail in future works.

The relatively weaker performance of GSIFN on CMU-MOSEI can be attributed to the extended sequence lengths of vision and audio modals, leading to excessive padding and semanticless information, which weakens GSIFN’s performance. Specifically, as described in Appendix B, the vision/audio sequence lengths for CMU-MOSI and CH-SIMS are 375/500 and 400/55, respectively, whereas the non-verbal modality sequence length for CMU-MOSEI reaches up to 500/500.

Additionally, the large variance in sequence length across modalities in CMU-MOSEI indicates an unstable data scale. This instability significantly impacts model performance. GSIFN did not pad or further process the semanticless information after filling to address sequence length differences, which affected and distracted the weight attention in GsiT’s fusion procedure and weakened the mLSTM-enhanced non-verbal modal’s final hidden state representation. As a result, GSIFN performs relatively weaker on CMU-MOSEI compared with CMU-MOSI and CH-SIMS.

Remarks. The sequence length of the text modality is less critical due to the padding mask tag, as BERT handles padded data well after masking.

The performance of our GSIFN model on fine-grained tasks such as MAE, Corr, and Acc-7, particularly on CMU-MOSEI and in real-world scenarios, could be further improved by the following approaches: (i) incorporating pre-training for unimodal data encoders for better alignment and representation, while ensuring efficiency; (ii) addressing over-redundant and semanticless information parameters in GsiT by padding non-verbal sequences; (iii) introducing advanced representation learning methods like contrastive learning and knowledge distillation to enhance encoder representation and robustness, thus improving the overall model.

References

- Alexei Baevski, Wei-Ning Hsu, Qiantong Xu, Arun Babu, Jiatao Gu, and Michael Auli. 2022. data2vec: A general framework for self-supervised learning in speech, vision and language. In *International Conference on Machine Learning, ICML 2022, 17-23 July 2022, Baltimore, Maryland, USA*, volume 162 of *Proceedings of Machine Learning Research*, pages 1298–1312. PMLR.
- Alexei Baevski, Yuhao Zhou, Abdelrahman Mohamed, and Michael Auli. 2020. wav2vec 2.0: A framework for self-supervised learning of speech representations. In *Advances in Neural Information Processing Systems 33: Annual Conference on Neural Information Processing Systems 2020, NeurIPS 2020, December 6-12, 2020, virtual*.
- AmirAli Bagher Zadeh, Paul Pu Liang, Soujanya Poria, Erik Cambria, and Louis-Philippe Morency. 2018. [Multimodal language analysis in the wild: CMU-MOSEI dataset and interpretable dynamic fusion graph](#). In *Proceedings of the 56th Annual Meeting of the Association for Computational Linguistics (Volume 1: Long Papers)*, pages 2236–2246, Melbourne, Australia. Association for Computational Linguistics.
- Tadas Baltrušaitis, Peter Robinson, and Louis-Philippe Morency. 2016. Openface: An open source facial behavior analysis toolkit. In *2016 IEEE Winter Conference on Applications of Computer Vision, WACV 2016, Lake Placid, NY, USA, March 7-10, 2016*, pages 1–10. IEEE Computer Society.
- Tadas Baltrušaitis, Amir Zadeh, Yao Chong Lim, and Louis-Philippe Morency. 2018. Openface 2.0: Facial behavior analysis toolkit. In *13th IEEE International Conference on Automatic Face & Gesture Recognition, FG 2018, Xi’an, China, May 15-19, 2018*, pages 59–66. IEEE Computer Society.
- Shaked Brody, Uri Alon, and Eran Yahav. 2022. How attentive are graph attention networks? In *The Tenth International Conference on Learning Representations, ICLR 2022, Virtual Event, April 25-29, 2022*. OpenReview.net.
- Junyoung Chung, Çağlar Gülçehre, KyungHyun Cho, and Yoshua Bengio. 2014. Empirical evaluation of gated recurrent neural networks on sequence modeling. *arXiv preprint arXiv:1412.3555*.
- Tri Dao and Albert Gu. 2024. Transformers are SSMs: Generalized models and efficient algorithms through structured state space duality. In *Proceedings of the 41st International Conference on Machine Learning*, volume 235 of *Proceedings of Machine Learning Research*, pages 10041–10071. PMLR.
- Gilles Degottex, John Kane, Thomas Drugman, Tuomo Raitio, and Stefan Scherer. 2014. COVAREP - A collaborative voice analysis repository for speech technologies. In *IEEE International Conference on Acoustics, Speech and Signal Processing, ICASSP 2014, Florence, Italy, May 4-9, 2014*, pages 960–964. IEEE.

- Jacob Devlin, Ming-Wei Chang, Kenton Lee, and Kristina Toutanova. 2019. [BERT: Pre-training of deep bidirectional transformers for language understanding](#). In *Proceedings of the 2019 Conference of the North American Chapter of the Association for Computational Linguistics: Human Language Technologies, Volume 1 (Long and Short Papers)*, pages 4171–4186, Minneapolis, Minnesota. Association for Computational Linguistics.
- Alexey Dosovitskiy, Lucas Beyer, Alexander Kolesnikov, Dirk Weissenborn, Xiaohua Zhai, Thomas Unterthiner, Mostafa Dehghani, Matthias Minderer, Georg Heigold, Sylvain Gelly, Jakob Uszkoreit, and Neil Houlsby. 2021. An image is worth 16x16 words: Transformers for image recognition at scale. In *9th International Conference on Learning Representations, ICLR 2021, Virtual Event, Austria, May 3-7, 2021*. OpenReview.net.
- Lingyong Fang, Gongshen Liu, and Ru Zhang. 2024. Multi-grained multimodal interaction network for sentiment analysis. In *IEEE International Conference on Acoustics, Speech and Signal Processing, ICASSP 2024, Seoul, Republic of Korea, April 14-19, 2024*, pages 7730–7734. IEEE.
- Ankita Gandhi, Kinjal Adhvaryu, Soujanya Poria, Erik Cambria, and Amir Hussain. 2023. Multimodal sentiment analysis: A systematic review of history, datasets, multimodal fusion methods, applications, challenges and future directions. *Inf. Fusion*, 91:424–444.
- Albert Gu and Tri Dao. 2023. Mamba: Linear-time sequence modeling with selective state spaces. *arXiv preprint arXiv:2312.00752*.
- Devamanyu Hazarika, Roger Zimmermann, and Soujanya Poria. 2020. MISA: modality-invariant and -specific representations for multimodal sentiment analysis. In *MM '20: The 28th ACM International Conference on Multimedia, Virtual Event / Seattle, WA, USA, October 12-16, 2020*, pages 1122–1131. ACM.
- S Hochreiter. 1997. Long short-term memory. *Neural Computation MIT-Press*.
- Kyeonghun Kim and Sanghyun Park. 2023. AOBERT: all-modalities-in-one BERT for multimodal sentiment analysis. *Inf. Fusion*, 92:37–45.
- Ronghao Lin and Haifeng Hu. 2024. Multi-task momentum distillation for multimodal sentiment analysis. *IEEE Trans. Affect. Comput.*, 15(2):549–565.
- Zhun Liu, Ying Shen, Varun Bharadhwaj Lakshminarasimhan, Paul Pu Liang, AmirAli Bagher Zadeh, and Louis-Philippe Morency. 2018. [Efficient low-rank multimodal fusion with modality-specific factors](#). In *Proceedings of the 56th Annual Meeting of the Association for Computational Linguistics (Volume 1: Long Papers)*, pages 2247–2256, Melbourne, Australia. Association for Computational Linguistics.
- Sijie Mai, Ying Zeng, Shuangjia Zheng, and Haifeng Hu. 2023. Hybrid contrastive learning of tri-modal representation for multimodal sentiment analysis. *IEEE Trans. Affect. Comput.*, 14(3):2276–2289.
- Bo Peng, Eric Alcaide, Quentin Anthony, Alon Albalak, Samuel Arcadinho, Stella Biderman, Huanqi Cao, Xin Cheng, Michael Chung, Leon Derczynski, Xingjian Du, Matteo Grella, Kranthi Gv, Xuzheng He, Haowen Hou, Przemyslaw Kazienko, Jan Koccon, Jiaming Kong, Bartłomiej Koptyra, Hayden Lau, Jiaju Lin, Krishna Sri Ipsit Mantri, Ferdinand Mom, Atsushi Saito, Guangyu Song, Xiangru Tang, Johan Wind, Stanisław Woźniak, Zhenyuan Zhang, Qinghua Zhou, Jian Zhu, and Rui-Jie Zhu. 2023a. [RWKV: Reinventing RNNs for the transformer era](#). In *Findings of the Association for Computational Linguistics: EMNLP 2023*, pages 14048–14077, Singapore. Association for Computational Linguistics.
- Junjie Peng, Ting Wu, Wenqiang Zhang, Feng Cheng, Shuhua Tan, Fen Yi, and Yansong Huang. 2023b. A fine-grained modal label-based multi-stage network for multimodal sentiment analysis. *Expert Syst. Appl.*, 221:119721.
- Korbinian Pöppel, Maximilian Beck, Markus Spanring, Andreas Auer, Oleksandra Prudnikova, Michael K Kopp, Günter Klambauer, Johannes Brandstetter, and Sepp Hochreiter. 2024. [xLSTM: Extended long short-term memory](#). In *First Workshop on Long-Context Foundation Models @ ICML 2024*.
- Alec Radford, Jong Wook Kim, Tao Xu, Greg Brockman, Christine McLeavey, and Ilya Sutskever. 2023. Robust speech recognition via large-scale weak supervision. In *International Conference on Machine Learning, ICML 2023, 23-29 July 2023, Honolulu, Hawaii, USA*, volume 202 of *Proceedings of Machine Learning Research*, pages 28492–28518. PMLR.
- Wasifur Rahman, Md Kamrul Hasan, Sangwu Lee, AmirAli Bagher Zadeh, Chengfeng Mao, Louis-Philippe Morency, and Ehsan Hoque. 2020. [Integrating multimodal information in large pretrained transformers](#). In *Proceedings of the 58th Annual Meeting of the Association for Computational Linguistics*, pages 2359–2369, Online. Association for Computational Linguistics.
- Steffen Schneider, Alexei Baevski, Ronan Collobert, and Michael Auli. 2019. wav2vec: Unsupervised pre-training for speech recognition. In *20th Annual Conference of the International Speech Communication Association, Interspeech 2019, Graz, Austria, September 15-19, 2019*, pages 3465–3469. ISCA.
- Yutao Sun, Li Dong, Shaohan Huang, Shuming Ma, Yuqing Xia, Jilong Xue, Jianyong Wang, and Furu Wei. 2023. Retentive network: A successor to transformer for large language models. *arXiv preprint arXiv:2307.08621*.
- Yao-Hung Hubert Tsai, Shaojie Bai, Paul Pu Liang, J. Zico Kolter, Louis-Philippe Morency, and Ruslan Salakhutdinov. 2019a. [Multimodal transformer](#)

- for unaligned multimodal language sequences. In *Proceedings of the 57th Annual Meeting of the Association for Computational Linguistics*, pages 6558–6569, Florence, Italy. Association for Computational Linguistics.
- Yao-Hung Hubert Tsai, Paul Pu Liang, Amir Zadeh, Louis-Philippe Morency, and Ruslan Salakhutdinov. 2019b. Learning factorized multimodal representations. In *7th International Conference on Learning Representations, ICLR 2019, New Orleans, LA, USA, May 6-9, 2019*. OpenReview.net.
- Ashish Vaswani, Noam Shazeer, Niki Parmar, Jakob Uszkoreit, Llion Jones, Aidan N. Gomez, Lukasz Kaiser, and Illia Polosukhin. 2017. Attention is all you need. In *Advances in Neural Information Processing Systems 30: Annual Conference on Neural Information Processing Systems 2017, December 4-9, 2017, Long Beach, CA, USA*, pages 5998–6008.
- Petar Velickovic, Guillem Cucurull, Arantxa Casanova, Adriana Romero, Pietro Liò, and Yoshua Bengio. 2018. Graph attention networks. In *6th International Conference on Learning Representations, ICLR 2018, Vancouver, BC, Canada, April 30 - May 3, 2018, Conference Track Proceedings*. OpenReview.net.
- Di Wang, Xutong Guo, Yumin Tian, Jinhui Liu, Lihuo He, and Xuemei Luo. 2023a. TETFN: A text enhanced transformer fusion network for multimodal sentiment analysis. *Pattern Recognit.*, 136:109259.
- Di Wang, Shuai Liu, Quan Wang, Yumin Tian, Lihuo He, and Xinbo Gao. 2023b. Cross-modal enhancement network for multimodal sentiment analysis. *IEEE Trans. Multim.*, 25:4909–4921.
- Lan Wang, Junjie Peng, Cangzhi Zheng, Tong Zhao, and Li'an Zhu. 2024. A cross modal hierarchical fusion multimodal sentiment analysis method based on multi-task learning. *Inf. Process. Manag.*, 61(2):103675.
- Zehui Wu, Ziwei Gong, Jaywon Koo, and Julia Hirschberg. 2024. Multimodal multi-loss fusion network for sentiment analysis. In *Proceedings of the 2024 Conference of the North American Chapter of the Association for Computational Linguistics: Human Language Technologies (Volume 1: Long Papers)*, pages 3588–3602, Mexico City, Mexico. Association for Computational Linguistics.
- Jianing Yang, Yongxin Wang, Ruitao Yi, Yuying Zhu, Azaan Rehman, Amir Zadeh, Soujanya Poria, and Louis-Philippe Morency. 2021. MTAG: Modal-temporal attention graph for unaligned human multimodal language sequences. In *Proceedings of the 2021 Conference of the North American Chapter of the Association for Computational Linguistics: Human Language Technologies*, pages 1009–1021, Online. Association for Computational Linguistics.
- Jiuding Yang, Yakun Yu, Di Niu, Weidong Guo, and Yu Xu. 2023. ConFEDE: Contrastive feature decomposition for multimodal sentiment analysis. In *Proceedings of the 61st Annual Meeting of the Association for Computational Linguistics (Volume 1: Long Papers)*, pages 7617–7630, Toronto, Canada. Association for Computational Linguistics.
- Wenmeng Yu, Hua Xu, Fanyang Meng, Yilin Zhu, Yixiao Ma, Jiele Wu, Jiyun Zou, and Kaicheng Yang. 2020. CH-SIMS: A Chinese multimodal sentiment analysis dataset with fine-grained annotation of modality. In *Proceedings of the 58th Annual Meeting of the Association for Computational Linguistics*, pages 3718–3727, Online. Association for Computational Linguistics.
- Wenmeng Yu, Hua Xu, Ziqi Yuan, and Jiele Wu. 2021. Learning modality-specific representations with self-supervised multi-task learning for multimodal sentiment analysis. In *Thirty-Fifth AAAI Conference on Artificial Intelligence, AAAI 2021, Thirty-Third Conference on Innovative Applications of Artificial Intelligence, IAAI 2021, The Eleventh Symposium on Educational Advances in Artificial Intelligence, EAAI 2021, Virtual Event, February 2-9, 2021*, pages 10790–10797. AAAI Press.
- Amir Zadeh, Minghai Chen, Soujanya Poria, Erik Cambria, and Louis-Philippe Morency. 2017. Tensor fusion network for multimodal sentiment analysis. In *Proceedings of the 2017 Conference on Empirical Methods in Natural Language Processing*, pages 1103–1114, Copenhagen, Denmark. Association for Computational Linguistics.
- Amir Zadeh, Paul Pu Liang, Navonil Mazumder, Soujanya Poria, Erik Cambria, and Louis-Philippe Morency. 2018. Memory fusion network for multi-sequential learning. In *Proceedings of the Thirty-Second AAAI Conference on Artificial Intelligence, (AAAI-18), the 30th innovative Applications of Artificial Intelligence (IAAI-18), and the 8th AAAI Symposium on Educational Advances in Artificial Intelligence (EAAI-18), New Orleans, Louisiana, USA, February 2-7, 2018*, pages 5634–5641. AAAI Press.
- Amir Zadeh, Rowan Zellers, Eli Pincus, and Louis-Philippe Morency. 2016. MOSI: multimodal corpus of sentiment intensity and subjectivity analysis in online opinion videos. *arXiv preprint arXiv:1606.06259*.
- Haoyu Zhang, Yu Wang, Guanghao Yin, Kejun Liu, Yuanyuan Liu, and Tianshu Yu. 2023. Learning language-guided adaptive hyper-modality representation for multimodal sentiment analysis. In *Proceedings of the 2023 Conference on Empirical Methods in Natural Language Processing*, pages 756–767, Singapore. Association for Computational Linguistics.
- Cangzhi Zheng, Junjie Peng, Lan Wang, Li'an Zhu, Jiatao Guo, and Zesu Cai. 2024. Frame-level non-verbal feature enhancement based sentiment analysis. *Expert Systems with Applications*, 258:125148.
- Daoming Zong, Chaoyue Ding, Baoxiang Li, Jiakui Li, Ken Zheng, and Qunyan Zhou. 2023. Acformer:

An aligned and compact transformer for multimodal sentiment analysis. In *Proceedings of the 31st ACM International Conference on Multimedia, MM 2023, Ottawa, ON, Canada, 29 October 2023- 3 November 2023*, pages 833–842. ACM.

A Experiment

A.1 Experiment Settings

Table 7: The hyperparameters of the main experiment.

Hyperparameter	CMU-MOSI	CMU-MOSEI	CH-SIMS
batch size	64	64	64
Learning Rate			
lr-bert	5×10^{-5}	5×10^{-6}	5×10^{-5}
lr-audio	5×10^{-5}	5×10^{-5}	5×10^{-5}
lr-video	5×10^{-5}	5×10^{-5}	5×10^{-5}
lr-other	5×10^{-4}	5×10^{-4}	1×10^{-4}
Weight Decay			
wd-bert	0.001	0.001	0.001
wd-audio	0.001	0.001	0.001
wd-video	0.001	0.001	0.001
wd-other	0.001	0.001	0.001
Model Hyper Parameter			
xlstm blocks	4	4	4
feature	128	128	128
heads	4	4	4
dropout	0.2	0.2	0.2

Table 8: The extractors of the main experiment.

Modal	CMU-MOSI	CMU-MOSEI	CH-SIMS
Text	bert-base-uncased	bert-base-uncased	bert-base-chinese
Vision	OpenFace	OpenFace	OpenFace2.0
Audio	COVAREP	COVAREP	LibROSA

In this section, we discuss the experiment settings. The hyperparameters of the main experiment are shown in Table 7. For further analysis experiments, the hyperparameters of MulT are the same as those of GSIFN in CMU-MOSI.

Following previous works (Peng et al., 2023b; Lin and Hu, 2024), the feature extraction tools of different modals in each dataset. BERT(Devlin et al., 2019) for text, OpenFace(Baltrusaitis et al., 2016) and OpenFace 2.0(Baltrusaitis et al., 2018) for vision, COVAREP(Degottex et al., 2014) and LibROSA for audio. The extractors for each dataset are shown in Table 8.

All experiments are performed on the platform equipped with the following hardware: GPU: Nvidia GeForce RTX 3060 12G; CPU: AMD Ryzen 9 5900X 12-Core Processor.

A.2 Further Ablation Study

In this section, experiments of further ablation study are performed and presented to fully analysis GSIFN. These experiments include Graph Structure Ablation, Fusion Modal Ablation, ULGM Modal Ablation, and Pretrained Language Model Ablation. Note that the multimodal representation (M) is used for the final classification task. In the original case, M is composed of unimodal text (T), vision (V), and audio (A).

Graph Structure Selection The structure of the graph has a significant impact on the performance of the model, so we conduct an ablation study on its graph structure. The structures include the original structure, structure-1, structure-2, structure-3, and self-only structure.

The graph structure of the three modals can only be constructed in four cases. Aiming for comparison, we design a self-only mask to interpret the influence of information disorder.

Original Structure: The original structure is defined as two opposing unidirectional ring graphs. They both realize cyclic all-modal-in-one fusion, which makes trimodal information fully interact in shared model weights. The structure is: $\{t \rightarrow v, v \rightarrow a, a \rightarrow t\}, \{a \rightarrow v, v \rightarrow t, t \rightarrow a\}$. The modal-wise IFMs are:

$$\begin{cases} \mathcal{M}_{inter}^{forward} = \begin{pmatrix} \mathcal{J}^{t,t} & \mathcal{O}^{t,v} & \mathcal{J}^{t,a} \\ \mathcal{J}^{v,t} & \mathcal{J}^{v,v} & \mathcal{O}^{v,a} \\ \mathcal{O}^{a,t} & \mathcal{J}^{a,v} & \mathcal{J}^{a,a} \end{pmatrix} \\ \mathcal{M}_{inter}^{backward} = \begin{pmatrix} \mathcal{J}^{t,t} & \mathcal{J}^{v,t} & \mathcal{O}^{a,t} \\ \mathcal{O}^{v,t} & \mathcal{J}^{v,v} & \mathcal{J}^{v,a} \\ \mathcal{J}^{a,t} & \mathcal{O}^{a,v} & \mathcal{J}^{a,a} \end{pmatrix} \end{cases} \quad (17)$$

Structure-1: Structure-1 realizes all-modal-in-one fusion, but the information passing is not cyclic. The structure is: $\{a \rightarrow v, v \rightarrow a, a \rightarrow t\}, \{v \rightarrow t, t \rightarrow v, t \rightarrow a\}$. The modal-wise IFMs are:

$$\begin{cases} \mathcal{M}_{inter}^{forward} = \begin{pmatrix} \mathcal{J}^{t,t} & \mathcal{J}^{t,v} & \mathcal{O}^{t,a} \\ \mathcal{J}^{v,t} & \mathcal{J}^{v,v} & \mathcal{O}^{v,a} \\ \mathcal{O}^{a,t} & \mathcal{J}^{a,v} & \mathcal{J}^{a,a} \end{pmatrix} \\ \mathcal{M}_{inter}^{backward} = \begin{pmatrix} \mathcal{J}^{t,t} & \mathcal{O}^{v,t} & \mathcal{J}^{t,a} \\ \mathcal{O}^{v,t} & \mathcal{J}^{v,v} & \mathcal{J}^{v,a} \\ \mathcal{O}^{a,t} & \mathcal{J}^{a,v} & \mathcal{J}^{a,a} \end{pmatrix} \end{cases} \quad (18)$$

Structure-2: Structure-2 realizes all-modal-in-one fusion, but the information passing is not cyclic.

The structure is: $\{v \rightarrow t, t \rightarrow v, v \rightarrow a\}$, $\{a \rightarrow t, t \rightarrow a, a \rightarrow v\}$. The modal-wise IFMs are:

$$\left\{ \begin{array}{l} \mathcal{M}_{inter}^{forward} = \begin{pmatrix} \mathcal{J}^{t,t} & \mathcal{O}^{t,v} & \mathcal{J}^{t,a} \\ \mathcal{O}^{v,t} & \mathcal{J}^{v,v} & \mathcal{J}^{v,a} \\ \mathcal{J}^{a,t} & \mathcal{O}^{a,v} & \mathcal{J}^{a,a} \end{pmatrix} \\ \mathcal{M}_{inter}^{backward} = \begin{pmatrix} \mathcal{J}^{t,t} & \mathcal{J}^{v,t} & \mathcal{O}^{t,a} \\ \mathcal{J}^{v,t} & \mathcal{J}^{v,v} & \mathcal{O}^{v,a} \\ \mathcal{O}^{a,t} & \mathcal{J}^{a,v} & \mathcal{J}^{a,a} \end{pmatrix} \end{array} \right. \quad (19)$$

Structure-3: Structure-3 realizes all-modal-in-one fusion, but the information passing is not cyclic. The structure is: $\{a \rightarrow v, v \rightarrow a, v \rightarrow t\}$, $\{a \rightarrow t, t \rightarrow a, t \rightarrow v\}$. The modal-wise IFMs are:

$$\left\{ \begin{array}{l} \mathcal{M}_{inter}^{forward} = \begin{pmatrix} \mathcal{J}^{t,t} & \mathcal{O}^{t,v} & \mathcal{J}^{t,a} \\ \mathcal{J}^{v,t} & \mathcal{J}^{v,v} & \mathcal{O}^{v,a} \\ \mathcal{J}^{a,t} & \mathcal{O}^{a,v} & \mathcal{J}^{a,a} \end{pmatrix} \\ \mathcal{M}_{inter}^{backward} = \begin{pmatrix} \mathcal{J}^{t,t} & \mathcal{J}^{v,t} & \mathcal{O}^{t,a} \\ \mathcal{O}^{v,t} & \mathcal{J}^{v,v} & \mathcal{J}^{v,a} \\ \mathcal{O}^{a,t} & \mathcal{J}^{a,v} & \mathcal{J}^{a,a} \end{pmatrix} \end{array} \right. \quad (20)$$

Additionally, we constructed a graph with only intra-mask which is diordered in multimodal temporal information.

Self-Only:

$$\mathcal{M}_{inter} = \begin{pmatrix} \mathcal{J}^{t,t} & \mathcal{O}^{t,v} & \mathcal{O}^{t,a} \\ \mathcal{O}^{v,t} & \mathcal{J}^{v,v} & \mathcal{O}^{v,a} \\ \mathcal{O}^{a,t} & \mathcal{O}^{a,v} & \mathcal{J}^{a,a} \end{pmatrix} \quad (21)$$

As shown in Table 9 part Graph Structure Ablation, the original structure is superior to other three theoretically feasible structures in all metrics. The four theoretically feasible structures are superior to the self-only structure, which is theoretically infeasible.

Fusion Modal Ablation To fully investigate the influence of the combined form of multimodal representation on the representation ability of the whole model, we design the Modal Ablation study, which contains the trimodal form: M(T, V, A); the bimodal forms: M(T, V), M(T, A), M(V, A); and the unimodal forms: M(T), M(V), M(A). Note that the structure of the model in the unimodal case is already missing, thus the graph-structured attention degenerates to naive multi-head self-attention.

As shown in Table 9 part Fusion Modal Ablation, modal combinations with text modal M(T, V, A), M(T, V), M(T, A), and M(T) have superior performance than those without text modal like M(V,

Table 9: Modal Ablation Study on CMU-MOSI. Note: F denotes finetuning pretrained language models, NF denotes not finetuning

Description	CMU-MOSI				
	Acc-2 \uparrow	F1 \uparrow	Acc-7 \uparrow	MAE \downarrow	Corr \uparrow
Graph Structure Ablation					
Original	85.0 / 86.0	85.0 / 86.0	48.3	0.707	0.801
Structure-1	82.4 / 84.0	82.3 / 84.0	46.5	0.712	0.792
Structure-2	83.8 / 85.7	83.7 / 85.6	46.1	0.731	0.796
Structure-3	83.4 / 85.1	83.3 / 85.1	45.5	0.727	0.793
Self-Only	81.6 / 83.2	81.7 / 83.3	43.3	0.750	0.791
Fusion Modal Ablation					
M(T,V,A)	85.0 / 86.0	85.0 / 86.0	48.3	0.707	0.801
M(T,V)	84.3 / 85.5	84.2 / 85.5	45.5	0.720	0.797
M(T,A)	84.3 / 85.7	84.3 / 85.7	47.2	0.704	0.800
M(V,A)	59.8 / 60.2	59.7 / 60.3	17.9	1.344	0.196
M(T)	83.1 / 84.8	83.0 / 84.7	47.5	0.715	0.786
M(V)	59.2 / 59.8	58.9 / 59.6	16.8	1.372	0.141
M(A)	60.4 / 61.3	59.0 / 60.0	21.3	1.322	0.236
ULGM Modal Ablation					
M+T+V+A	85.0 / 86.0	85.0 / 86.0	48.3	0.707	0.801
M+T+V	84.4 / 85.7	84.3 / 85.7	44.5	0.742	0.742
M+T+A	83.9 / 85.7	83.7 / 85.6	46.1	0.731	0.796
M+V+A	83.8 / 85.2	83.8 / 85.3	44.6	0.748	0.794
M+T	83.4 / 85.7	83.3 / 85.6	45.0	0.731	0.796
M+V	83.5 / 85.4	83.5 / 85.4	45.8	0.724	0.801
M+A	82.5 / 84.6	82.4 / 84.6	46.1	0.709	0.800
M	83.4 / 84.8	83.4 / 84.8	46.7	0.711	0.801
Pretrained Language Model Ablation					
BERT(F)	85.0 / 86.0	85.0 / 86.0	48.3	0.707	0.801
BERT(NF)	83.8 / 85.7	83.7 / 85.6	46.1	0.731	0.796

A). For those who have text modal, trimodal combination M(T, V, A) performs better than bimodal combination M(T, V) and M(T, A). In bimodal combinations, audio modal plays a relatively more important role than vision modal in multimodal fusion. In unimodal cases, only text modal has superior performance than vision and audio.

ULGM Modal Ablation In the Self-Supervised Learning Framework, multimodal (M) is used for classification, and unimodal text (T), vision (V), and audio (A) are used to generate unimodal labels in ULGM to ensure that the model learns a robust representation of the multimodal data.

To fully analyze the importance of each modal in the model, we design ULGM modal ablation experiment. The forms include ULGM with three modals: M+T+V+A, ULGM with two modals: M+T+V, M+T+A, M+V+A, ULGM with one modal: M+T, M+V, M+A, and without ULGM: M.

As shown in Table 9 part ULGM Modal Ablation, take M+T as an example, compared with M+T+V and M+T+A, M+T performs weaker in coarse-grained tasks (Acc-2, F1). The binary clas-

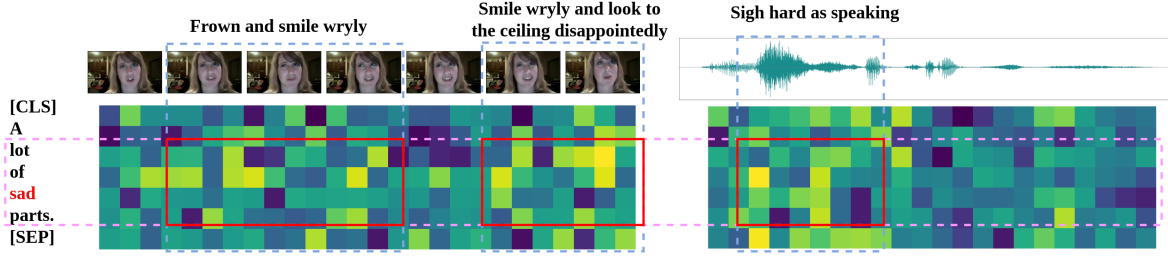


Figure 3: Example of Alignment.

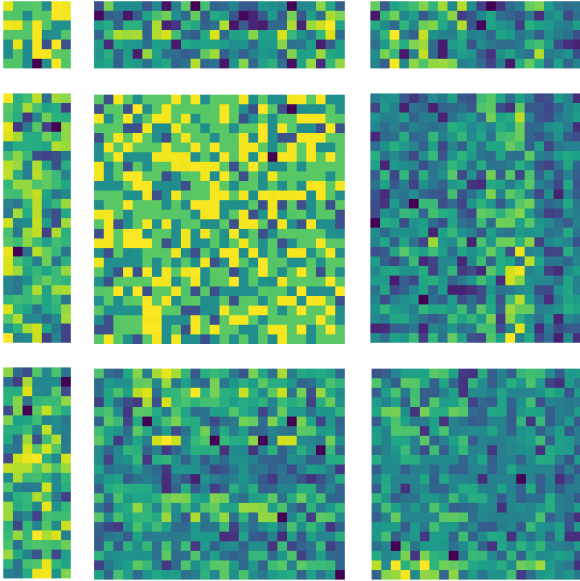


Figure 4: Attention map split by interlaced masks.

sification performance of GSIFN is affected by the number of modals in ULGM. However, take M as an example, the performance of M in fine-grained tasks (Acc-7, MAE) is superior to M+A, M+T, etc. Among all of the cases, M+T+V+A achieves the best performance. Therefore, ULGM promotes the coarse-grained capability of GSIFN, GsiT boosts the fine-grained capability of GSIFN.

Pretrained Language Model Ablation The experiment on whether or not finetuning BERT is shown in Table 9, part Pretrained Language Model Ablation. The result shows that BERT finetuning is quite useful to GSIFN.

A.3 Alignment

Specifically, a real-time example of a complete adjacency matrix (attention map) of the original structure is shown in Figure 4.

An analysis example of the alignment efficiency of GSIFN is shown in Figure 3. We choose bimodal combinations of vision-to-text and audio-to-text as

examples, these two groups are produced from two different MGEs. As can be seen from Figure 3, GSIFN effectively and comprehensively composes the semantics of the three modals together.

B Datasets

Table 10: Dataset basic information, sample distribution statistics, and data forms for MSA datasets. Note: for part Sample Distribution Statistics, data is in format negative (< 0)/neutral (= 0)/positive (> 0) sentiment intensity. For part Data Forms, data is in format text / vision / audio.

Description	CMU-MOSI	CMU-MOSEI	CH-SIMS
Basic Information			
Language	English	English	Chinese
Unimodal Labels	None	None	T,V,A
Sample Distribution Statistics			
Train	552/53/679	4,738/3,540/8,084	742/207/419
Validation	92/13/124	506/433/932	248/69/139
Test	379/30/227	1,350/1,025/2,284	248/69/140
Total	2,199	22,856	2,281
Data Forms			
Sequence Length(Max)	50/375/500	50/500/500	39/400/55
Average Length(Train)	14/42/38	24/94/149	17/22/158
Average Length(Validation)	14/43/37	25/100/156	17/21/154
Average Length(Test)	16/52/49	25/95/153	17/21/157
Length Variance(Train)	66/927/805	148/5,115/8,105	53/116/6,050
Length Variance(Validation)	63/983/658	145/4,626/7,401	48/101/5,358
Length Variance(Test)	91/1,773/1,526	141/5,254/8,325	51/108/5,647
Feature Dimension	768/20/5	768/35/74	768/709/33

A brief introduction to the three chosen datasets is shown in Table 10. The detailed descriptions are as follows.

CMU-MOSI(Zadeh et al., 2016): The CMU-MOSI is a widely used dataset for human multimodal sentiment analysis, containing 2,198 short monologue video clips. Each clip is a single-sentence utterance expressing the speaker’s opinion on a topic like movies. The utterances are manually annotated with a continuous opinion score ranging from -3 to +3, where -3 represents highly negative, -2 negative, -1 weakly negative, 0 neutral, +1 weakly positive, +2 positive, and +3 highly positive.

CMU-MOSEI (Bagher Zadeh et al., 2018): CMU-MOSEI is an improved version of CMU-MOSI, containing 23,453 annotated video clips (approximately 10 times more than CMU-MOSI) from 5,000 videos, involving 1,000 different speakers and 250 distinct topics. The dataset also features a larger number of discourses, samples, speakers, and topics compared to CMU-MOSI. The range of labels for each discourse remains consistent with CMU-MOSI.

CH-SIMS (Yu et al., 2020): The CH-SIMS dataset includes the same modalities as CMU-MOSI: audio, text, and video, collected from 2281 annotated video segments. It features data from TV shows and movies, making it culturally distinct and diverse. Additionally, CH-SIMS provides multiple labels for the same utterance based on different modalities, adding an extra layer of complexity and richness to the data.

C Baselines

The introduction to baseline models is as follows.

TFN(Zadeh et al., 2017): The Tensor Fusion Network (TFN) uses modal embedding subnetwork and tensor fusion to learn intra- and inter-modal dynamics.

MFN(Zadeh et al., 2018): The Memory Fusion Network (MFN) explicitly accounts for both interactions in a neural architecture and continuously models them through time.

MuIT(Tsai et al., 2019a): The Multimodal Transformer (MuIT) uses a cross-modal Transformer based on cross-modal attention to make modal translation.

MTAG(Yang et al., 2021): The Modal-Temporal Attention Graph (MTAG) is a graph neural network model that incorporates modal attention mechanisms and dynamic pruning techniques to effectively capture complex interactions across modes and time, achieving a parametrically efficient and interpretable model.

MISA(Hazarika et al., 2020): The Modality-Invariant and -Specific Representations (MISA) project representations into modal-specific and modal-invariant spaces and learn distributional similarity, orthogonal loss, reconstruction loss, and task prediction loss.

Self-MM(Yu et al., 2021): Learning Modal-Specific Representations with Self-Supervised Multi-Task Learning (Self-MM) designs a multi- and a uni- task to learn inter-modal consistency and

intra-modal specificity.

HyCon-BERT(Mai et al., 2023): proposes a novel multimodal representation learning framework HyCon based on contrastive learning, designed with three types of losses to comprehensively learn inter-modal and intra-modal dynamics in both supervised and unsupervised ways.

TETFN(Wang et al., 2023a): Text Enhanced Transformer Fusion Network (TETFN) strengthens the role of text modes in multimodal information fusion through text-oriented cross-modal mapping and single-modal label generation, and uses Vision-Transformer pre-training model to extract visual features.

ConFEDE(Yang et al., 2023): Contrastive Feature Decomposition (ConFEDE) constructs a unified learning framework that jointly performs contrastive representation learning and contrastive feature decomposition to enhance the representation of multimodal information.

MMIN(Fang et al., 2024): Multi-modal Interaction Network (MMIN) is an advanced multimodal sentiment analysis model that combines a coarse-grained interaction network (CIN) and a fine-grained interaction network (FIN). Adversarial learning and sparse attention mechanisms are used to capture complex interactions between different modals and reduce redundant and irrelevant information.

MTMD(Lin and Hu, 2024): Multi-Task Momentum Distillation (MTMD) treats the modal learning process as multiple subtasks and knowledge distillation between teacher network and student network effectively reduces the gap between different modes, and uses momentum models to explore mode-specific knowledge and learn robust multimodal representations through adaptive momentum fusion factors.

D Aggregation of Modal Subgraphs

D.1 How to Aggregate Subgraphs?

In this section, we offer the derivation of graph aggregation from vertex to subgraph.

Vertex Aggregation Assuming a set of vertex features, $\mathcal{V} = \{v_1, v_2, \dots, v_N\}$, $v_i \in \mathbb{R}^D$, where N is the number of vertices, and D is the feature dimension in each vertex.

From previous works (Velickovic et al., 2018; Brody et al., 2022), the GAT is defined as follows. GAT performs self-attention on the vertices, which is a shared attentional mechanism $a : \mathbb{R}^{D'} \times \mathbb{R}^D \rightarrow$

\mathbb{R} computes attention coefficients. Before that, a shared linear transformation, parameterized by a weight matrix, $\mathbf{W} \in \mathbb{R}^{D' \times D}$.

$$e^{i,j} = a(\mathbf{W}v_i, \mathbf{W}v_j) = (\mathbf{W}v_i) \cdot (\mathbf{W}v_j)^\top \quad (22)$$

$e^{i,j}$ indicates the importance of vertex j 's features to vertex i . In the most general formulation, the model allows a vertex to attend to every other vertex, which drops all structural information. GAT injects the graph structure into the mechanism by performing masked attention: it only computes $e^{i,j}$ for vertex $j \in \mathcal{N}_i$, where \mathcal{N}_i is some neighbor of vertex i in the graph. To make coefficients easily comparable across different vertices, GAT normalizes them across all choices of j using the softmax function (\mathcal{S}):

$$\alpha^{i,j} = \mathcal{S}_j(e^{i,j}) = \frac{\exp(e^{i,j})}{\sum_{k \in \mathcal{N}_i} \exp(e^{i,k})} \quad (23)$$

Unlike GAT, whose attention mechanism a is a single-layer feedforward neural network, we directly employ a multi-head self-attention mechanism as the aggregation algorithm.

Therefore, the final output features for every vertex is defined as follows.

$$\bar{v}_i = \sum_{j \in \mathcal{N}_i} \alpha^{i,j} \mathbf{W}v_j \quad (24)$$

Then, we extend the mechanism to multi-head attention. The concatenation operation is defined as \parallel . K refers to the number of heads in multi-head self-attention.

$$\bar{v}_i = \parallel_{k=1}^K \sum_{j \in \mathcal{N}_i} \alpha_k^{i,j} \mathbf{W}_k v_j \quad (25)$$

From Vertex to Subgraph Assuming two sets of vertices $\mathcal{V}_i = \{v_1^i, v_2^i, \dots, v_{N_i}^i\}$, $v_m^i \in \mathbb{R}^{D_i}$ and $\mathcal{V}_j = \{v_1^j, v_2^j, \dots, v_{N_j}^j\}$, $v_n^j \in \mathbb{R}^{D_j}$. Where $N_{\{i,j\}}$ is the number of vertices of $\mathcal{V}_{\{i,j\}}$, $D_{\{i,j\}}$ is the feature dimension of each vertex in $\mathcal{V}_{\{i,j\}}$.

Then, apply the GAT algorithm on v_m^i and v_n^j . Instead of a shared linear transformation, we use two weight matrices, query weight $\mathbf{W}_q^m \in \mathbb{R}^{D'_i \times D_i}$ and key weight $\mathbf{W}_k^n \in \mathbb{R}^{D'_j \times D_j}$.

$$e^{m,n} = a(\mathbf{W}_q^m v_m^i, \mathbf{W}_k^n v_n^j) \quad (26)$$

$$\alpha^{m,n} = \mathcal{S}_n(e^{m,n}) = \frac{\exp(e^{m,n})}{\sum_{l \in \mathcal{N}_n} \exp(e^{m,l})} \quad (27)$$

After that, the final output feature for v_m^i is computed. The value weight $\mathbf{W}_v^m \in \mathbb{R}^{D'_i \times D_i}$ is applied to transform v_n^j :

$$\bar{v}_m^i = \parallel_{l=1}^L \sum_{n \in \mathcal{N}_m} \alpha_l^{m,n} \mathbf{W}_{v_l}^m v_n^j \quad (28)$$

In the subgraph aspect, we assume that \mathcal{N}_m includes all the vertices in subgraph \mathcal{V}_j . The current attention coefficient matrix is a vector \mathcal{G}^m , it can be regarded as a graph aggregated from \mathcal{V}_j to v_m^i . The key, value weight for \mathcal{V}_j is represented as $\mathcal{W}_{\{k,v\}} \in \mathbb{R}^{N_j \times D'_j \times D_j}$. Then, the aggregation can be defined as follows:

$$e^m = a(\mathbf{W}_q^m v_m^i, \mathcal{W}_k \mathcal{V}_j), \quad \mathcal{G}^m = \mathcal{S}(e^m) \quad (29)$$

$$\bar{v}_m^i = \parallel_{l=1}^L (\mathcal{G}_l^m \mathcal{W}_{v_l} \mathcal{V}_j) \quad (30)$$

Then, apply the algorithm defined by Equation 28, 29, 30 to all the vertices in \mathcal{V}_i . The aggregation form is now vertex set to vertex set, thus, we regard the vertex sets as subgraphs and vertex-to-vertex aggregation is transformed into subgraph aggregation. Also, the attention coefficient matrix e is transformed as a directional subgraph adjacency matrix \mathcal{E} . The query weight for \mathcal{V}_i is represented as \mathcal{W}_q .

$$\mathcal{E}^{i,j} = a(\mathcal{W}_q \mathcal{V}_i, \mathcal{W}_k \mathcal{V}_j), \quad \mathcal{G}^{i,j} = \mathcal{S}(\mathcal{E}^{i,j}) \quad (31)$$

$$\bar{\mathcal{V}}_i = \parallel_{l=1}^L (\mathcal{G}_l^{i,j} \mathcal{W}_{v_l} \mathcal{V}_j) \quad (32)$$

Now the aggregation procedure is equal to the multi-head cross-attention mechanism in MulT (Tsai et al., 2019a). Also, it is equal to the multi-head cross-attention in the decoder of vanilla Transformer (Vaswani et al., 2017).

Multimodal Subgraph Aggregation Take \mathcal{V}_i and \mathcal{V}_j , where $\{i, j\} \in \{t, v, a\}$ two modal sequences as an example, which is regarded as two vertex sets. Assuming that the unidirectional subgraph is constructed by the two modal vertex sequences, the adjacency matrix weight aggregation process of the corresponding subgraph is as follows.

$$\mathcal{E}^{i,j} = (\mathcal{W}_q \mathcal{V}_i) \cdot (\mathcal{W}_k \mathcal{V}_j)^\top \quad (33)$$

Then apply the softmax function, which is defined as \mathcal{S} .

$$\mathcal{G}^{i,j} = \mathcal{S}(\mathcal{E}^{i,j}) \quad (34)$$

Finally, some of the edges in the subgraph are randomly masked which is realized by the dropout operation implemented on the adjacency matrix, which is defined as \mathcal{D} .

$$\mathcal{G}_{dropout}^{i,j} = \mathcal{D}(\mathcal{G}^{i,j}) \quad (35)$$

where \mathcal{D} denotes the dropout function.

After the aggregation, the fusion process is started, which is regarded as the directional information fusion procedure from \mathcal{V}_j to \mathcal{V}_i .

$$\bar{\mathcal{V}}_i = \mathcal{G}_{dropout}^{i,j} \mathcal{W}_v \mathcal{V}_j \quad (36)$$

Then we extend the above operation globally as follows:

$$\mathcal{G} = \mathcal{S} \circ \mathcal{D}(\mathcal{A}) \quad (37)$$

$$\bar{\mathcal{V}}_m = \mathcal{G} \mathcal{W}_v \mathcal{V}_m \quad (38)$$

Where \circ represents the function composition operation. Note: \mathcal{A} is defined in Equation 5

Constructed graph structure in Equation 37 is actually unstructured at all, it loses sight of the separated modal-wise temporal features of the concatenated sequence which makes the sequence disordered. What is more, it over-fuses the inter-modal information, confuses inter-modal information and the intra-modal information, and leaves way too much fine-grained information unconsidered. Thus, we propose the Interlaced-Mask mechanism to further address these problems.

D.2 Why the Interlaced Mask?

Take the first block row in \mathcal{A} as an example, which is $\mathbf{BR} = [\mathcal{E}^{t,t}, \mathcal{E}^{t,v}, \mathcal{E}^{t,a}]$. Knowing that $\mathcal{V}_m = [\mathcal{V}_t; \mathcal{V}_v; \mathcal{V}_a]^\top$. Then the $\mathcal{E}^{t,t}$ is aggregated by \mathcal{V}_t of \mathcal{V}_m itself, $\mathcal{E}^{t,v}$ is aggregated by \mathcal{V}_t and \mathcal{V}_v , $\mathcal{E}^{t,a}$ is aggregated by \mathcal{V}_t and \mathcal{V}_a . And as defined in Equation 31, 32, the direction of aggregation of $\mathcal{E}^{i,j}$ is from j to i .

If the final output feature computational is performed without interlaced mask. It has to be noted that aggregation in this case is only performed on text modal t .

$$\bar{\mathcal{V}}_t = \mathbf{BR} \cdot (\mathcal{W}_v \mathcal{V}_m) \quad (39)$$

As shown in Figure 5. When we only mask one or two blocks (subgraphs), vertex sequences of different modals are considered to be the same sequence because they are spliced together. Thus making the temporal information disordered, which is not advisable.

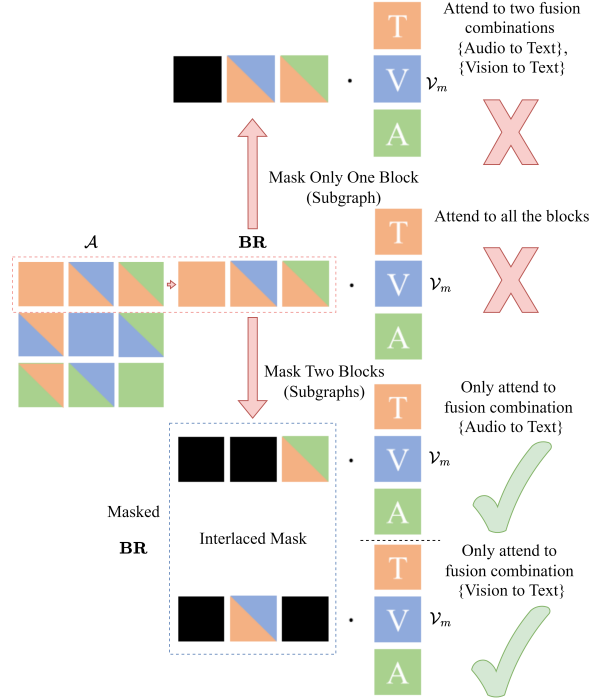


Figure 5: Example of to explain the necessity of interlaced mask.

E Architecture Comparison

A detailed explanation of the architecture difference between MulT and GsiT is shown in Figure 6.

GsiT uses only 3 Transformers for multimodal fusion, as contrast, MulT and other multimodal Transformer-based fusion methods use at least 9 Transformers for a complete fusion procedure. It achieves an all-modal-in-one fusion method without information disorder, which ensures the outstanding performance and efficiency of GSIFN.

F Algorithms

F.1 Interlaced Mask Generation Algorithm

Algorithm 1 Interlaced Mask Generation

Input: Segmentation of the length of three-modal sequence $seg = \{T_t, T_v, T_a\}$, Mode of the mask generation $mode \in \{inter, intra\}$, Direction of fusion procedure $dir \in \{forward, backward\}$;
Output: The generated mask of appointed mode and direction;

- 1: Let $\{l_t, l_v, l_a\} = seg$
- 2: Define segments $s1 = (0, l_t)$, $s2 = (l_t, l_t + l_v)$, $s3 = (l_t + l_v, l_t + l_v + l_a)$
- 3: Let $l_{sum} = l_t + l_v + l_a$
- 4: Initialize an empty list \mathcal{M}_{list}

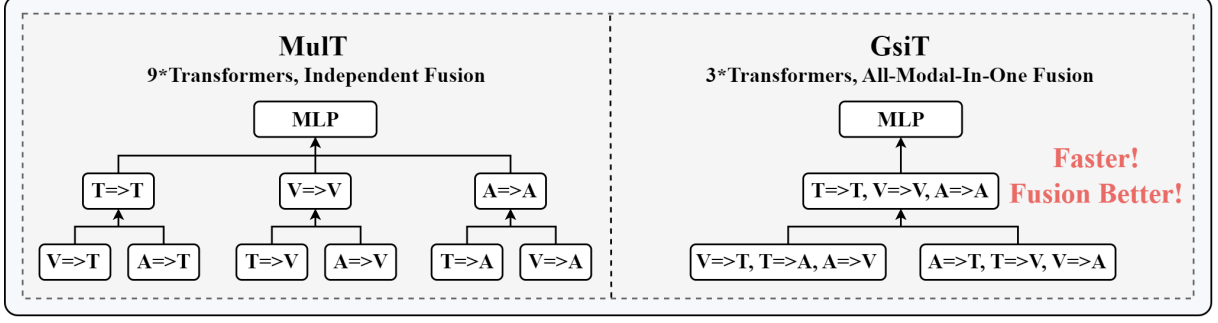


Figure 6: Architecture comparison between Mult and GsiT.

```

5: for each  $i$  in  $[0, 1, 2]$  do
6:   for each element in  $seg[i]$  do
7:     Initialize  $m_{row}$  as a tensor of ones with
       size  $l_{sum}$ 
8:     if  $i == 0$  then
9:       Set  $m_{row}[0 : s1[1]] = 0$ 
10:      if  $mode == inter$  then
11:        if  $dir == forward$  then
12:          Set  $m_{row}[s3[0] :] = 0$ 
13:        else if  $dir == backward$  then
14:          Set  $m_{row}[s2[0] : s2[1]] = 0$ 
15:        end if
16:      end if
17:    else if  $i == 1$  then
18:      Set  $m_{row}[s2[0] : s2[1]] = 0$ 
19:      if  $mode == inter$  then
20:        if  $dir == forward$  then
21:          Set  $m_{row}[0 : s1[1]] = 0$ 
22:        else if  $dir == backward$  then
23:          Set  $m_{row}[s3[0] :] = 0$ 
24:        end if
25:      end if
26:    else if  $i == 2$  then
27:      Set  $m_{row}[s3[0] : s3[1]] = 0$ 
28:      if  $mode == inter$  then
29:        if  $dir == forward$  then
30:          Set  $m_{row}[s2[0] : s2[1]] = 0$ 
31:        else if  $dir == backward$  then
32:          Set  $m_{row}[0 : s1[1]] = 0$ 
33:        end if
34:      end if
35:    end if
36:    Append  $m_{row}$  to  $\mathcal{M}_{list}$ 
37:  end for
38: end for
39: if  $mode == inter$  then
40:   Let  $\mathcal{M} = \text{Stack}(\mathcal{M}_{list})$ 
41:   return  $\text{GenerateMask}(\mathcal{M})$ 
42: else if  $mode == intra$  then

```

```

43:   return  $\text{GenerateMask}(|\text{Stack}(\mathcal{M}_{list}) - 1|)$ 
44: end if

```

The detailed generation method of interlaced mask for not only the forward and backward inter-fusion but also the intra-enhancement is shown in the algorithm table above. It is of vital importance for our model to accurately construct the graph structure of the concatenated sequence list. The masks could be constructed during the initialization procedure.

F.2 Extended Long Short Term Memory with Matrix Memory

$$C_t = f_t C_{t-1} + i_t v_t k_t^\top \quad (40)$$

$$n_t = f_t n_{t-1} + i_t k_t \quad (41)$$

$$h_t = o_t \odot \tilde{h}_t, \quad \tilde{h}_t = \frac{C_t q_t}{\max\{|n_t^\top q_t|, 1\}} \quad (42)$$

$$q_t = W_q X_t + b_q \quad (43)$$

$$k_t = \frac{1}{\sqrt{d}} W_k X_t + b_k \quad (44)$$

$$v_t = W_v X_t + b_v \quad (45)$$

$$i_t = \exp(\tilde{i}_t), \quad \tilde{i}_t = w_i^\top X_t + b_i \quad (46)$$

$$f_t = \sigma(\tilde{f}_t) \text{OR} \exp(\tilde{f}_t), \quad \tilde{f}_t = w_f^\top X_t + b_f \quad (47)$$

$$o_t = \sigma(\tilde{o}_t), \quad \tilde{o}_t = W_o X_t + b_o \quad (48)$$

The definition of mLSTM (Pöppel et al., 2024) can be described as the above equation group, while the detailed architecture is shown in Figure 7.

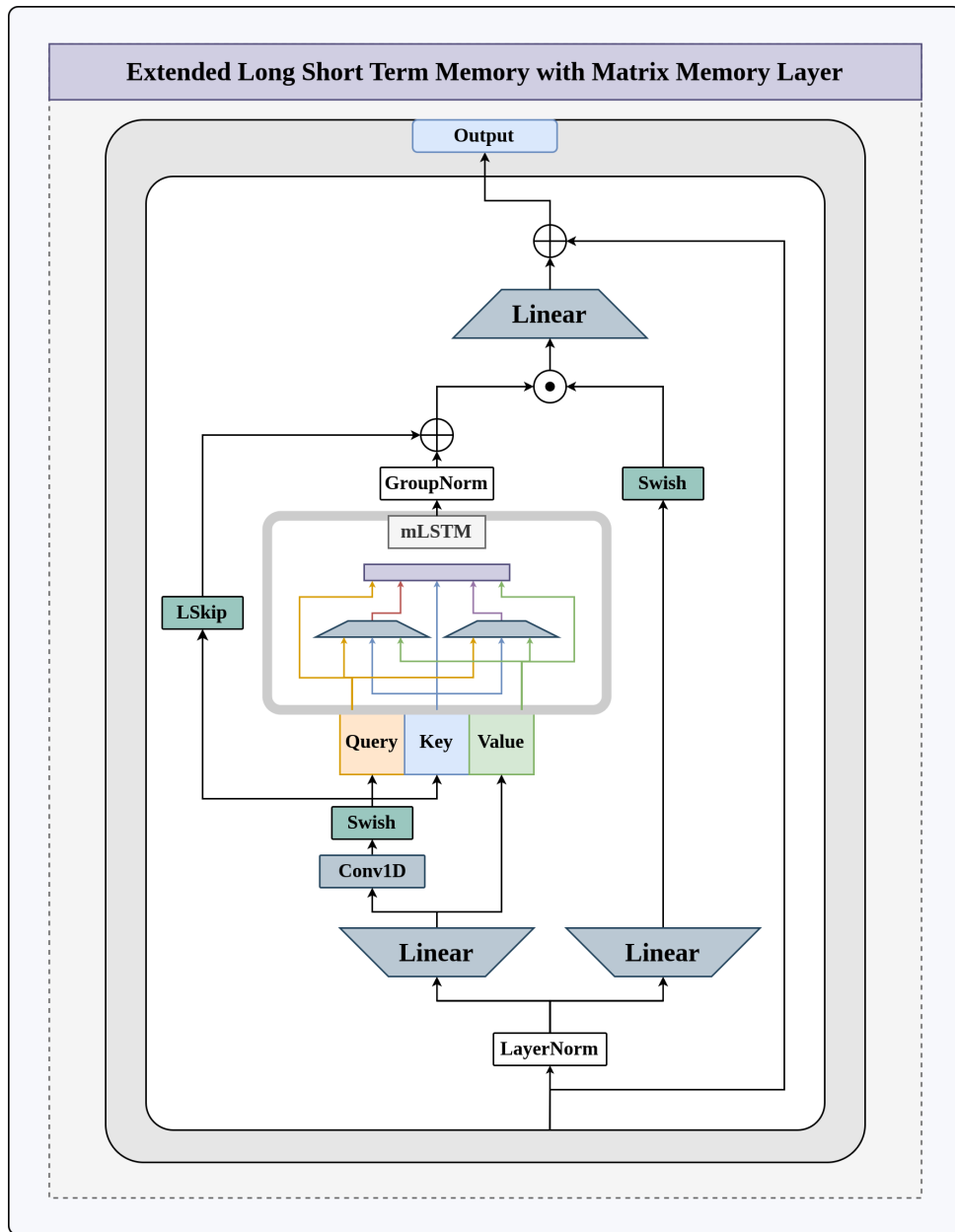


Figure 7: Architecture of Parallelized Extended LSTM with Matrix Memory (mLSTM).